ELSEVIER

Materials Science and Engineering B 114–115 (2004) 82–87

MATERIALS SCIENCE & ENGINEERING B

www.elsevier.com/locate/mseb

Atomistic modeling of defect evolution in Si for amorphizing and subamorphizing implants

Pedro Lopez*, Lourdes Pelaz, Luis A. Marqués, Ivan Santos, Maria Aboy, Juan Barbolla

Departamento de Electricidad y Electrónica, Universidad de Valladolid, Campus Miguel Delibes s/n, 47011 Valladolid, Spain

Abstract

Solid phase epitaxial regrowth of pre-amorphizing implants has received significant attention as a method to achieve high dopant activation with minimal diffusion at low implant temperatures and suppress channelling. Therefore, a good understanding of the amorphization and regrowth mechanisms is required in process simulators. We present an atomistic amorphization and recrystallization model that uses the interstitial–vacancy (I–V) pair as a building block to describe the amorphous phase. I–V pairs are locally characterized by the number of neighbouring I–V pairs. This feature captures the damage generation and the dynamical annealing during ion implantation, and also explains the annealing behaviour of amorphous layers and amorphous pockets.
© 2004 Elsevier B.V. All rights reserved.

Keywords: Amorphization model; Recrystallization; Amorphous pockets

1. Introduction

Ion implantation is the standard technique used to introduce dopants for the fabrication of Si integrated circuits. However, this process produces considerable damage in the lattice, going from point defects or point defect clusters surrounded by crystalline silicon, to continuous amorphous layers. From the point of view of applications, the amorphization of a silicon near-surface zone can occur during the fabrication of Si devices because of the high implantation doses used to achieve high dopant concentrations. On the other hand, the pre-amorphization of the wafer prior to a very low energy dopant implantation, has several advantages for the fabrication of ultra-shallow junctions, suppressing channelling and leading to a high activation of the dopants with lower temperatures anneals [1]. The drawback of this technique is that, after regrowth, end of range defects remain beyond the initial amorphous/crystalline (a/c) interface. During subsequent annealings they contribute to dopant clustering, cause transient enhanced diffusion, and may increase the junction leakage if they are not completely removed.

While there is still some controversy about the mechanisms of amorphization through homogeneous [2] or heterogeneous [3] nucleation, there is a clear need for a good understanding of amorphization mechanisms and for the development of predictive models, as it was stated in the 2001 edition of the International Technology Roadmap for Semiconductors [4]: "more detailed understanding of implant damage, amorphization and subsequent recrystallization is important, as these phenomena can critically affect dopant profiles [...] extensive research and model development needs to be started immediately to develop improved models for damage creation and annealing, and for temperature-dependent implantation".

One of the most commonly used amorphization models is based on a critical defect concentration, i.e., the region being implanted turns amorphous when this critical defect concentration is exceeded [5]. However, the critical point defect density is not accurately known. Values ranging from 10^{21} to 10^{23} cm^{-3} have been reported. Variations in the critical defect density lead to different depths of the a/c interface, which affects strongly the amount of residual damage after recrystallization. The variation in the threshold defect concentration value reflects the resistance of damage to anneal. Thus, elevated implant temperatures need larger values of generated defects to make up for the annihilation of some of them.

* Corresponding author.
E-mail address: pedrol@ele.uva.es (P. Lopez).

0921-5107/$ – see front matter © 2004 Elsevier B.V. All rights reserved.
doi:10.1016/j.mseb.2004.07.040

In this work, we use an atomistic model to describe defect generation during ion implantation going from point defects to continuous amorphous layers. Dynamical annealing during the implant process is taken into account. We study the behaviour of amorphous layers as well as isolated amorphous pockets (a-pockets), explaining the most relevant features concerning the different activation energies observed in the regrowth of the damage.

2. Simulation model

Our atomistic simulations are based on the following scheme: implantation cascades are simulated with binary collision computer code MARLOWE [6], and the coordinates of the resulting Si self-interstitials and vacancies are transferred to the kinetic nonlattice Monte Carlo diffusion code DADOS [7]. In the nonlattice kinetic Monte Carlo technique, only the atoms belonging to point or extended defects are simulated. Clusters of point defects are formed when the mobile point defects jump within the capture radius of other point defects or pre-existing clusters. We consider that defects interact when they are within second-neighbour distance of each other. The dissolution of the defects occurs by the emission of a point defect at a rate determined by their binding energy. The energies used in Monte Carlo simulations are obtained from ab initio calculations or estimated by fitting experimental data [8,9]. The surface is considered as an efficient sink for point defects. After each cascade annealing at the implant temperature is carried out during a time defined by the dose rate of the implant. This takes into account the dynamical anneal during the implant and thus, the influence of implant parameters on damage accumulation.

We have recently implemented a fully atomistic amorphization and recrystallization model in this kinetic Monte Carlo scheme [10], using the interstitial–vacancy (I–V) pair as the basic defect to describe the amorphous phase. Marqués et al. [11] have proved that Si amorphization can be modeled by I–V pair accumulation. We assume that Si interstitials and vacancies generated in each implantation cascade interact and form the metastable ‘bond defect’ or ‘I–V pair’, instead of undergoing instantaneous annihilation. This defect has no excess or deficit of atoms, but introduces disorder in the lattice with the five- and seven-membered rings characteristic of the amorphous phase [11,12]. In our model each I–V pair is characterized locally by the number of neighbouring I–V pairs. This allows the model to capture any damage topology that may arise from irradiation cascades, as well as the characteristic regrowth behaviour observed in the experiments, as we will see later. The recombination rate of the I–V pair decreases as the number of neighbouring I–V pairs increases. We assign an activation energy of 0.43 eV to the isolated I–V pair (0 neighbours), according to MD calculations [11]. The activation energy of the recrystallization velocity of a planar crystal–amorphous interface, 2.7 eV [13], provides us with another parameter to characterize the recrystallization rate of I–V pairs with about half of the total coordination number. I–V pairs embedded into an amorphous matrix (completely surrounded by neighbouring I–V pairs, and thus with full coordination) have an activation energy of 5 eV, coincident with the experimentally observed activation energy for crystal nucleation in amorphous Si [14]. Intermediate coordination numbers have interpolated activation energies. When the Si interstitials and vacancies produced during the implantation interact with an I–V pair, they are called as “amorphous interstitials” or “amorphous vacancies” and they correspond to local excess or deficit of atoms that may exist within amorphous regions. These defects are moved only as the regrowth of the amorphous region proceeds. Their energy decreases with the number of I–V neighbours and, therefore, they tend to be within the amorphous region. In this way defects are effectively swept towards inner zones as the regrowth takes place. Molecular dynamics (MD) simulations showed that after regrowth of a-pockets only the net excess or deficit of atoms remains [15].

3. Results and discussion

The local characterization of each I–V pair in our model by the number of neighbouring I–V pairs, allows us to simulate any damage topology going from isolated I–V pairs to complete amorphous layers, including amorphous pockets of any size and geometry. We have studied the resulting damage configurations after amorphizing and subamorphizing implants, their behaviour upon annealing, and also analysed the role that size and geometry play on the evolution of amorphous pockets.

3.1. Annealing of amorphous pockets

One of the main difficulties in characterizing irregular amorphous regions is the lack of a well-defined activation energy for the regrowth process, unlike the recrystallization of a planar amorphous interface. Amorphous zones with similar starting sizes show very different recrystallization rates, indicating that size is not the key factor of their regrowth. Video recordings of the evolution of a-pockets with time [16] show that the recovery of small amorphous zones is a two-step process, in which there is an initial fast shrinkage followed by a plateau and a latter fast regrowth that leads to the complete recrystallization of the a-pocket. The regrowth of an isolated amorphous region seems to require a triggering event that produces a rapid shrinkage of the a-pocket, as it has been observed both in experiments and in detailed MD simulations [17]. The combination of fast shrinkages and plateaux and the lack of an exponential decay, shows that the annealing behaviour of a-pockets is not controlled by a single activation energy. In addition different activation energies were measured for the onset of an amorphous layer created by different ions [18]. MD simulations [17] have also revealed

the difficulty in characterizing the activation energy for the regrowth of a-pockets.

These behaviours can be easily explained by considering that the regrowth is governed by the local rearrangement of the atoms. In our model the activation energy of any I–V pair is locally defined depending on the number of neighbouring I–V pairs. This helps explaining the different recrystallization rates of a-pockets with apparently the same size. In the model a-pockets are considered agglomerates of I–V pairs. Though the surface of an a-pocket is usually very irregular, (with valleys and peaks), we have used two regular geometries: a sphere and a cube, to analyse the recrystallization of a-pockets (Fig. 1). In an irregular surface there are I–V pairs with few neighbouring I–V pairs which recombine fast, shortening the lifetime of the a-pocket (Fig. 1a). On the contrary, all the I–V pairs at the surface of a sphere-shaped a-pocket see the same number of neighbouring I–V pairs (Fig. 1b). Their activation energy is higher and therefore the recrystallization slower. The regrowth of this kind of interface, in which there is a large number of I–V pairs with the same number of neighbouring I–V pairs, follows a triggering event scheme. At the beginning all the I–V pairs at the interface have the same probability of recombining. Once one of them has already recombined, it leaves a "hole" (crystalline atom) in the interface, and the I–V pairs surrounding this "hole" are the next ones to recombine because they have fewer neighbouring I–V pairs. As they have a lower activation energy, their recombination takes place faster than that of the first I–V pair. The fast shrinkages followed by plateaux experimentally observed may represent the evolution of irregular interfaces.

The size of the a-pocket plays also an important role on the recrystallization. Going on with the example of the spherical a-pocket, the I–V pairs at the interface of a bigger a-pocket have more neighbouring I–V pairs and therefore undergo a slower recrystallization. It is important to note that in this model a planar interface is a particular case of an amorphous pocket, where the I–V pairs at the interface have a well-defined number of I–V neighbours. In fact, experiments have pointed out the similar annealing and structural features of a-pockets and continuous amorphous layers [19]. In this way, our model allows the recrystallization of any amorphous region to be simulated in a consistent manner.

Fig. 2 shows the evolution during annealing at 400 °C of two a-pockets of the same size, 511 I–V pairs each, but with different geometries: a cube and a sphere. It is clearly shown, that despite their identical size, the cube-like a-pocket takes half the time to completely regrowth. Regions of faster decay followed by others with slow decay are observed as in experiments [16]. Because of its geometry, there is some I–V pairs, the ones in the corners and in the edges, with few neighbouring I–V pairs and therefore a faster recombination occurs. In both cases there is an initial fast decay caused by the annihilation of some external I–V pairs until a more compact structure is formed. The final fast shrinkage is due to the fact that once the size is small, even compact geometries have few neighbours.

3.2. Amorphizing and subamorphizing implants

3.2.1. Subamorphizing implant

Depending on the implant parameters, such as ion mass, dose rate and implant temperature, generated I–V pairs may recombine or accumulate leading to the formation of small amorphous pockets and finally extended amorphous regions. In Fig. 3 we show several snapshots of the annealing of the damage produced by a Si 5 keV 10^{14} cm^{-2} 5×10^{13} cm^{-2} s^{-1} implant performed at room temperature, which corresponds to a subamorphizing implant. The first snapshot shows the damage generated by the ion

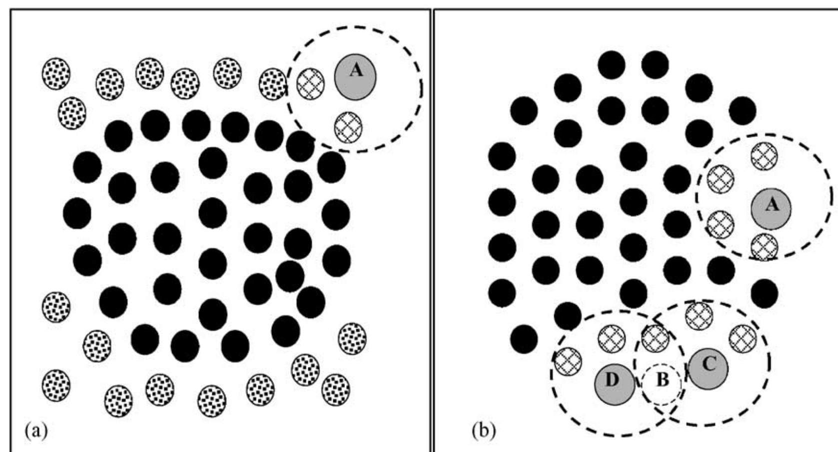

Fig. 1. Scheme of the damage topology of two a-pockets. Each circle represents an I–V pair. Hatched circles are the neighbouring I–V pairs considered. (a) Projection of a cube-like a-pocket. I–V pairs in the corners (A) will recombine first since they see fewer I–V neighbours. The a-pocket will undergo a fast shrinkage until a more compact structure (solid circles) is reached. (b) Projection of a spherical a-pocket. Initially all the I–V pairs in the interface (A) have the same probability of recombining because they have the same number of neighbouring I–V pairs. Once one of them has already recombined (B), there are some I–V pairs (C and D) with fewer I–V neighbours (three neighbours each) and therefore they will be the next ones to recombine.

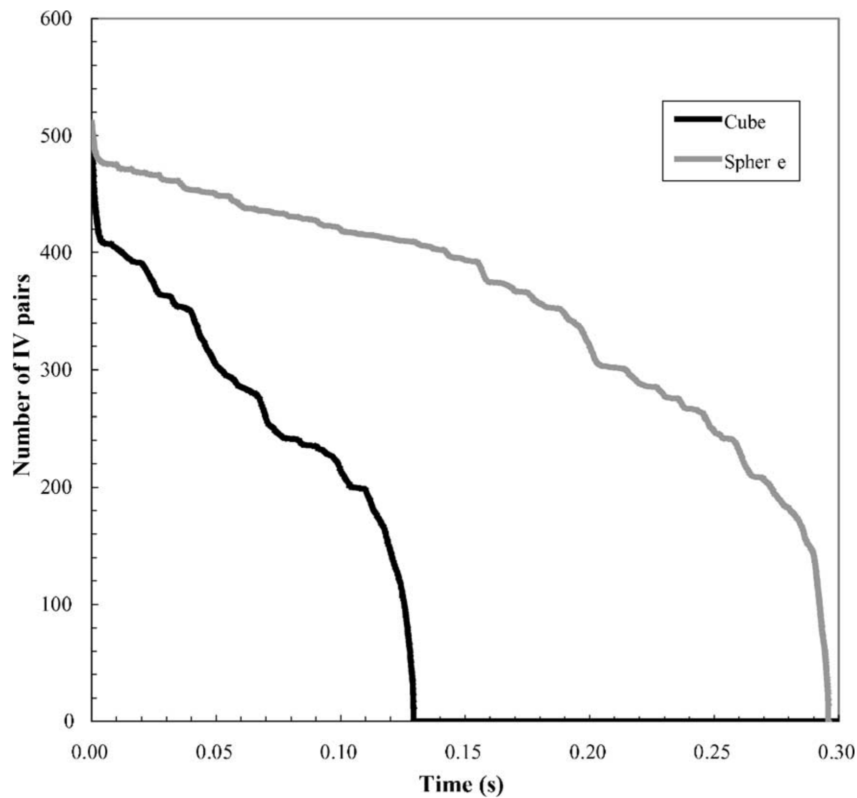

Fig. 2. Number of I–V pairs of two amorphous pockets when annealed at 400 °C. Both a-pockets have initially the same size (511 I–V pairs) but different geometries: a cube and a sphere. The plot shows the fast decays and the plateaux characteristics of the annealing of isolated amorphous regions.

implantation: I–V pairs and amorphous pockets, Si interstitials and vacancies can be observed. The amorphous pockets are not fully connected and there are still crystalline regions between them. As the sample is annealed and the regrowth takes place small amorphous pockets recombine, leaving behind the local excess (interstitials) or deficit (vacancies) of atoms contained within those a-pockets (Fig. 3b). When no a-pockets are left (Fig. 3c), excess Si interstitials and vacancies are still present in all the implanted region. The diffusion of these point defects leads to the interaction of some Si interstitials with vacancies forming I–V pairs which, isolated, recombine soon. The remaining Si interstitials evolve to extended defects, such as 311s (Fig. 3d). Thus, extended defects are present over the implanted region, and concentrate slightly deeper than the projected range, in the region where most of the implanted ions are stopped. The number of interstitials in these extended defects fits the implant dose, giving validity to the +1 model. According to this model the large number of interstitials and vacancies produced during the ion implantation form first I–V pairs, but they recombine upon annealing and only the unpaired interstitials displaced by the incident ions remain.

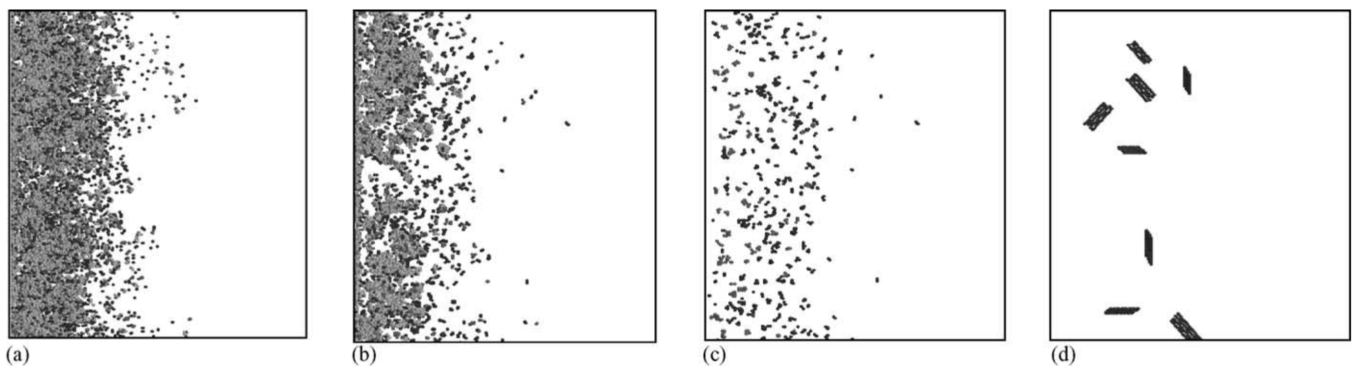

Fig. 3. Damage evolution of a 5 keV 10^{14} cm^{-2} Si implant at a dose rate of 5×10^{13} cm^{-2} s^{-1}, corresponding to a subamorphizing implant. Light points represent I–V pairs. Dark points correspond to Si interstitials and vacancies. (a) Damage after implantation at room temperature. (b) Damage annealing at 550 °C. (c) Defects remaining after regrowth. (d) 311 defects resulting after annealing at 800 °C.

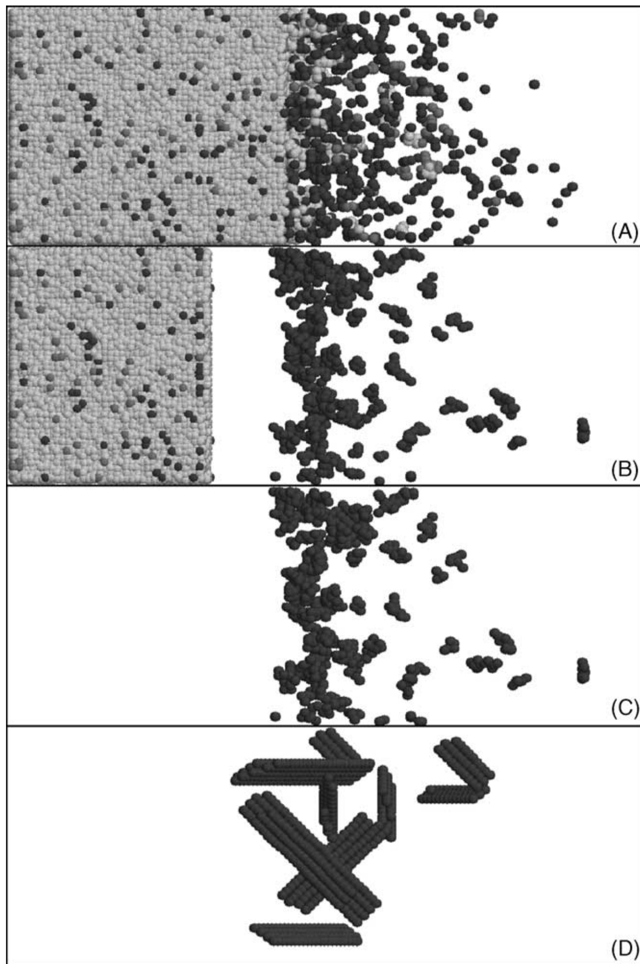

Fig. 4. Damage evolution of a 5 keV 10^{15} cm^{-2} Si implant at a dose rate of 5 $\times$ 10^{14} cm^{-2} s^{-1}, by which a continuous amorphous layer has been formed. Light points represent I–V pairs. Dark points correspond to Si interstitials and vacancies. (a) Damage after implantation at room temperature. (b) Damage annealing at 550 °C. (c) Defects remaining after regrowth. (d) 311 defects resulting after annealing at 800 °C.

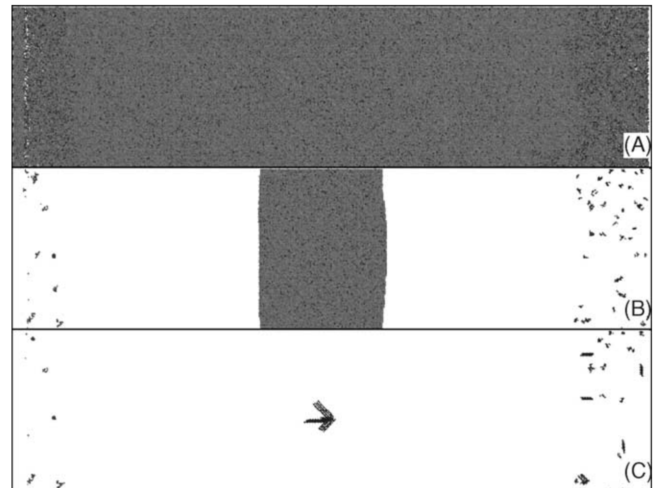

Fig. 5. Evolution upon annealing of a buried amorphous layer produced by a Si 80 keV 10^{15} cm^{-2} implant at a dose rate of 10^{12} cm^{-2} s^{-1}. Light points represent I–V pairs. Dark points correspond to Si interstitials and vacancies. (a) Damage after implantation at room temperature. (b) Damage annealing at 550 °C. The a-layer regrowths from both interfaces. (c) Extended defects remaining after annealing at 800 °C. Vacancy clusters are predominant near the surface. A band of defects have formed at the position where the two regrowing interfaces merge.

3.2.2. Amorphizing implant

The annealing behaviour of a fully amorphizing implant is significantly different from the previous case, as it is shown in the set of snapshots of Fig. 4. In this simulation we have implanted at room temperature 10^{15} cm^{-2} Si at 5 keV at a dose rate of 5 $\times$ 10^{14} cm^{-2} s^{-1}. For these implant parameters a continuous amorphous layer has been formed, that extends from the surface to approximately 17 nm. Beyond the a/c interface the scene is similar to that of the subamorphizing implant (Fig. 4a), with the existence of a-pockets and Si interstitial and vacancy clusters. A-pockets recrystallize faster than the planar interface since the I–V pairs in their surface are surrounded by fewer neighbouring I–V pairs. The regrowth of the continuous amorphous layer takes longer and proceeds layer by layer. When an I–V pair of a planar amorphous interface recombines, its neighbouring I–V pairs have one neighbour less, and therefore they are the next ones to recombine. As the a/c interface moves, point defects within the amorphous region are swept towards the surface (Fig. 4b). Since the amorphous layer extends to the surface the excess of deficit of atoms are annihilated there. When the regrowth finishes, the initially amorphous region is now a crystalline zone free of defects (Fig. 4c). Only the residual damage beyond the initial a/c interface evolves upon annealing to extended defects (Fig. 4d) until they finally dissolve with longer annealing times. Note that in this case the region of more damage (near the projected range) is the one that amorphizes. Residual defects are significantly deeper than the projected range of the implanted ions and only a fraction of the implanted dose remains.

It is also worth analysing the behaviour of a buried amorphous layer. For this reason we have implanted 10^{15} cm^{-2} Si at 80 keV at a dose rate of 10^{12} cm^{-2} s^{-1}. The evolution of this layer upon annealing is shown in Fig. 5. The continuous amorphous layer shrinks from both sides as the regrowth takes place. Si interstitials and vacancies within the amorphous layer are swept towards the centre of the layer from both interfaces. Since there is no free surface to accommodate the residual damage, at the end of the process a band of defects are formed at the position where the two regrowing interfaces merge, as also observed in experiments [20]. Due to the “mismatch” between the two merging interfaces, other defects (not considered in this model) may be formed in addition to Si-interstitial defects.

4. Conclusions

We have developed a fully atomistic model to describe amorphization and regrowth in silicon. The model success-

fully explains the most intriguing features of annealing behaviour, such as the differences observed in the annealing of a-pockets regarding their geometry. The same consistent model is used to describe damage evolution in subamorphizing and amorphizing implants at an atomistic level. Dynamical annealing effects during ion implantation [10] are also captured by the model.

Acknowledgements

This work has been supported by the Spanish DGICYT under project BFM 2001-2250 and the Consejeria de Educacion y Cultura de la JCYL under project VA-010/02.

References

[1] M.Y. Tsai, B.G. Streetman, J. Appl. Phys. 50 (1979) 183.
[2] J.R. Dennis, E.B. Hale, J. Appl. Phys. 49 (1978) 1119.
[3] F.F. Morehead, B.L. Crowder, Radiat. Eff. 6 (1970) 27.
[4] International Technology Roadmap for Semiconductors, 2001 ed., http://public.itrs.net/.
[5] G. Hobler, G. Otto, Mater. Sci. Semicond. Process. 6 (2003) 1.
[6] M.T. Robinson, I.M. Torrens, Phys. Rev. B 9 (1974) 5008.
[7] M. Jaraiz, L. Pelaz, J.E. Rubio, J. Barbolla, G.H. Gilmer, D.J. Eaglesham, H.-J. Gossman, J.M. Poate, Mater. Res. Soc. Symp. Proc. 532 (1998) 43.
[8] D.J. Eaglesham, P.A. Stolk, H.-J. Gossmann, J.M. Poate, Appl. Phys. Lett. 65 (1994) 2305.
[9] N.E.B. Cowern, et al., Phys. Rev. Lett. 82 (1999) 4460.
[10] L. Pelaz, L.A. Marqués, M. Aboy, J. Barbolla, Appl. Phys. Lett. 82 (2003) 2038.
[11] L.A. Marqués, L. Pelaz, J. Hernandez, J. Barbolla, G.H. Gilmer, Phys. Rev. B 64 (2001) 045214.
[12] M. Tang, L. Colombo, J. Zhu, T. Diaz de la Rubia, Phys. Rev. B 55 (1997) 4279.
[13] G.L. Olson, J.A. Roth, Mater. Sci. Rep. 3 (1988) 78.
[14] Y. Masaki, P.G. LeComber, A.G. Fitzgerald, J. Appl. Phys. 74 (1993) 129.
[15] T. Diaz de la Rubia, G.H. Gilmer, Phys. Rev. Lett. 74 (1995) 2507.
[16] S.E. Donnelly, R.C. Birtcher, V.M. Vishnyakov, G. Carter, Appl. Phys. Lett. 82 (2003) 1860.
[17] M.-J. Caturla, T. Diaz de la Rubia, L.A. Marqués, Phys. Rev. B 54 (1996) 16683.
[18] R.D. Goldberg, J.S. Williams, R.G. Elliman, Nucl. Instrum. Methods Phys. Res., Sect. B 106 (1995) 242.
[19] A. Battaglia, F. Priolo, E. Rimini, G. Ferla, Appl. Phys. Lett. 56 (1990) 2622.
[20] K. Sadana, M. Stratham, J. Washburn, G.R. Booker, J. Appl. Phys. 51 (1980) 5718.